Nanoscale

PAPER

View Article Online
View Journal | View Issue

Cite this: *Nanoscale*, 2015, **7**, 14305

Efficient red luminescence from organic-soluble Au_{25} clusters by ligand structure modification†

Ammu Mathew,[a] Elizabeth Varghese,[a] Susobhan Choudhury,[b] Samir Kumar Pal[b] and T. Pradeep*[a]

Received 26th May 2015,
Accepted 21st July 2015

DOI: 10.1039/c5nr03457d

www.rsc.org/nanoscale

An efficient method to enhance visible luminescence in a visibly non-luminescent organic-soluble 4-(*tert* butyl)benzyl mercaptan (SBB)-stabilized Au_{25} cluster has been developed. This method relies mainly on enhancing the surface charge density on the cluster by creating an additional shell of thiolate on the cluster surface, which enhances visible luminescence. The viability of this method has been demonstrated by imparting red luminescence to various ligand-protected quantum clusters (QCs), observable to the naked eye. The bright red luminescent material derived from $Au_{25}SBB_{18}$ clusters was characterized using UV-vis and luminescence spectroscopy, TEM, SEM/EDS, XPS, TG, ESI and MALDI mass spectrometry, which collectively proposed an uncommon molecular formula of $Au_{29}SBB_{24}S$, suggested to be due to different stapler motifs protecting the Au_{25} core. The critical role of temperature on the emergence of luminescence in QCs has been studied. The restoration of the surface ligand shell on the Au_{25} cluster and subsequent physicochemical modification to the cluster were probed by various mass spectral and spectroscopic techniques. Our results provide fundamental insights into the ligand characteristics determining luminescence in QCs.

Introduction

Luminescent noble metal quantum clusters (QCs) with intriguing physicochemical properties such as near infrared (NIR) emission, low toxicity, good biocompatibility, *etc*. have shown significant promise in biolabeling, imaging and sensing.[1–4] Consequently, various attempts have been made to synthesize QCs with visible luminescence. The photophysical properties of QCs largely depend on their structure and chemical environments such as the cluster core size, protecting ligands, solvents, surface charge, *etc*.[5] A better understanding of the origin of luminescence in such clusters (whether from core or staple atoms) can lead to new approaches for the design and synthesis of clusters with strong luminescence and improved quantum yields (QY). Though size-dependent emission, ranging from UV to IR, is a commonly observed phenomenon in such clusters;[6] a change in visible emission might not always be a direct indication of change in cluster core size.[7] A recent study suggests that nonluminescent oligomeric Au(I)–glutathione complexes can generate very strong luminescence upon aggregation. An aggregation-induced emission (AIE) mechanism was proposed for the synthesis of a highly luminescent Au cluster.[8] Also similar-sized clusters protected by different ligands often lead to clusters with varying QYs suggesting the strong ligand effects on luminescence.[9–11] Therefore, appropriate ligands are chosen for specific applications.[2,3,12] Recently thermal treatment of mercaptosuccinic acid and tiopronin protected Au clusters was found to enhance the quantum efficiency of NIR emission significantly.[13] However, the vast majority of QCs showing visible luminescence are water-soluble and are prepared in polar solvents with hydrophilic ligands.[5,7,14–17] Visible luminescence in hydrophobic ligand-stabilized QCs, in nonpolar organic media, is rare.[18] For organic-soluble clusters, emission is typically in the NIR region with weak QYs ($\sim 10^{-4}$ and 10^{-5}).[9,19–21] Such materials capable of dissolving in non-polar and moderately polar solvents could be of great interest for their applications in biomedicine and imaging.[22–25] Among the various nonpolar organic ligand-modified QCs known in the literature, $Au_{25}SR_{18}$ (SR denotes the thiolate ligand) with a known crystal structure,[26–28] is well-studied. Though various aspects of Au_{25} such as catalytic,[29–32] electrochemical,[33] magnetic,[28,34,35] chiral,[36] alloying,[37–41] ligand exchange,[42–44] supramolecular functionalization,[45] *etc*.,[2,20,46] have been explored, the absence of strong visible luminescence in the organic

[a]*DST Unit of Nanoscience (DST UNS) and Thematic Unit of Excellence, Department of Chemistry, Indian Institute of Technology Madras, Chennai 600036, India. E-mail: pradeep@iitm.ac.in; Fax: +91-44 2257-0545*

[b]*Department of Chemical Biological & Macromolecular Sciences, S. N. Bose National Centre for Basic Sciences, Block JD, Sector III, Salt Lake, Kolkata 700098, India*

†Electronic supplementary information (ESI) available: Additional data on characterization of red luminescent Au_{29} QC and comparison with parent $Au_{25}SBB_{18}$ are given. See DOI: 10.1039/c5nr03457d

phase hinders their applications in areas such as sensing and imaging. Even though fine-tuning of surface characteristics has been exploited for modifying the physicochemical properties of QCs,[9,13,16,45] new approaches to make significant modifications in the physical and chemical properties of QCs without disrupting the cluster core are highly desirable. Herein, we describe an efficient strategy to increase the visible luminescence of a visibly non-luminescent and organic thiol-stabilized QC by increasing its surface charge density while preserving its stability. This was achieved by making an additional shell of Au(I)SR thiolate on a visibly non-luminescent Au_{25} precursor *via* mild thermal annealing.

Results and discussion

For this study, we chose Au_{25} QCs protected by a 4-(*tert*-butyl)-benzyl mercaptan (SBB) ligand, synthesized and characterized in our previous work,[45] as they exhibited well-defined optical and mass spectral features. The optical absorption spectrum of $Au_{25}SBB_{18}$ solution (black trace in Fig. 1A) revealed discrete molecule-like features, characteristic of the cluster. The stability of the cluster was confirmed using optical absorption measurements. Fig. S1A in the ESI† shows the comparison of the UV-vis absorption spectra of as-prepared Au_{25} (black trace) and the same after 2 months (red trace) of synthesis. Moreover, the $Au_{25}SBB_{18}$ QCs were stable against thiol-induced etching of the core even in the presence of ten-fold excess BBSH present in solution at room temperature (Fig. S1B†).

Au_{25} clusters stabilized by hydrophobic ligands such as phenylethanethiol (PET), dodecanethiol (DDT), BBSH, *etc.*, have a weak emission (10^{-5}–10^{-7} QY) in the visible region and a relatively stronger emission in the NIR region (10^{-3} QY). The fluorescence is influenced by various factors such as the nature of the protecting ligands[9,10] as well as their charge states.[9,47,48] $Au_{25}SBB_{18}$ QCs also showed a strong luminescence in the NIR region in comparison with the visible region (blue and green traces in Fig. S1C†), an expanded version (125 000 times) of the original spectrum is also shown for comparison) and no luminescence was observable to the naked eye (see photographs shown in the inset of Fig. S1C†). Interestingly, heating of purified $Au_{25}SBB_{18}$ clusters with Au(I)SBB thiolate (1 : 1 Au^{3+} and BBSH thiol) for 2 h enhanced the visible luminescence significantly (Fig. S2A†), along with increasing amount of thiolate in the solution. This could possibly be due to the surface charge modification of the QCs.[8,9,49,50] The intensity of luminescence reached a maximum after the addition of 0.05 mL of thiolate to Au_{25} (1 mL, 0.1 mM) (Fig. S2B†). No further enhancement in the intensity was observed, suggesting the saturation of the cluster surface by the thiolate shell that can directly interact with the cluster core. Moreover, heating the purified cluster solution at 55 °C for a period of 24 h with additionally added Au(I)SBB thiolate was identified to yield a maximum emission intensity (Fig. S2C†). These experiments are described in more detail in the ESI.† The samples were cooled for 3 h before the PL measurement. A bar diagram shown in Fig. S2D† illustrates the improved luminescence obtained by the addition of thio-

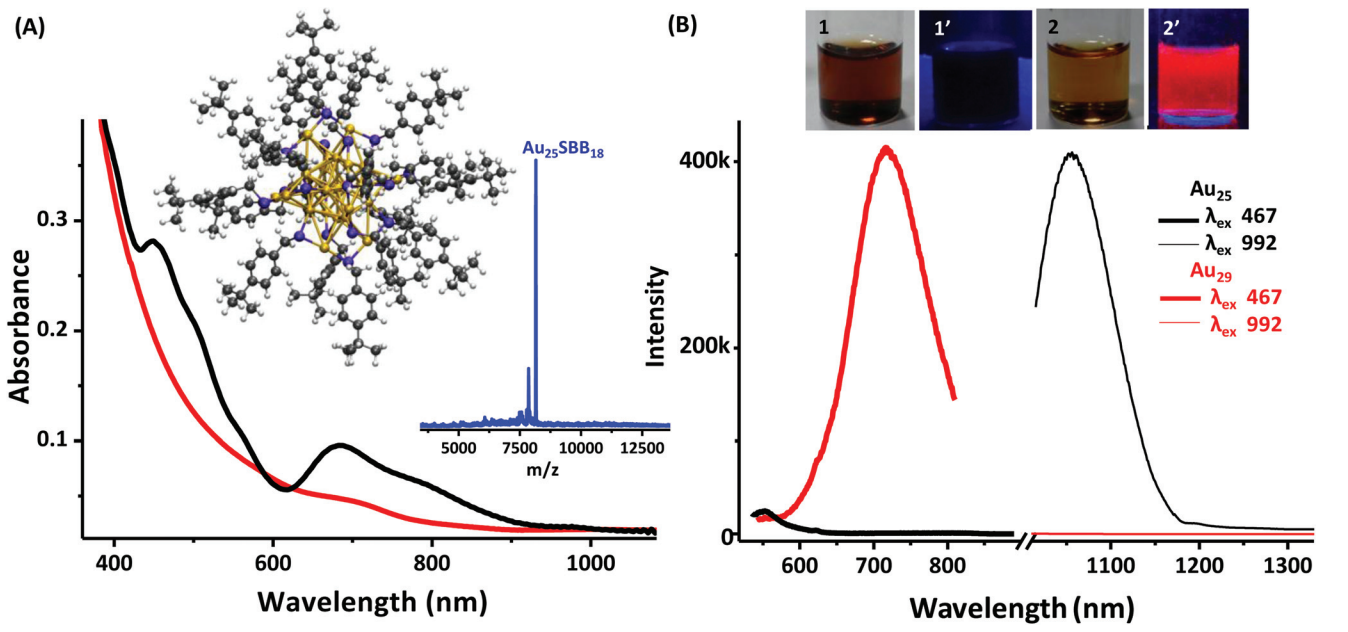

Fig. 1 Comparison of the UV-vis absorption spectrum (A) and emission spectra (B) of $Au_{25}SBB_{18}$ (black trace) and the resultant red luminescent cluster (red trace) in the visible (thick lines) and NIR range (thin lines), at excitation wavelengths of 467 and 992 nm, respectively. The inset of (A) shows a visualization of the DFT-optimized structure of $Au_{25}SBB_{18}$. Gold, sulfur, carbon and hydrogen atoms are shown in gold, blue, dark gray, and light grey, respectively. The MALDI mass spectrum of parent $Au_{25}SBB_{18}$ clusters showing a peak at *m/z* 8152 Da is also shown in the inset. Photographs of the Au_{25} (1, 1′) and red luminescent (2, 2′) clusters in visible light (1, 2) and UV light (1′, 2′), respectively are shown in the inset of (B).

late to pure Au_{25} QCs with heating for 24 h (green bars), in comparison with that without heating for 24 h (red bars). Such a thiolate addition to previously prepared red luminescent clusters resulted only in the quenching of cluster emission due to dilution of the solution (blue bars). Based on the above observation, we optimized the conditions to obtain red luminescent clusters in high yield, which involved the following steps: (i) synthesis of the precursor $Au_{25}SBB_{18}$ QCs, (ii) thermal treatment of Au_{25} QCs for 24 h and addition of definite amounts of Au(I)SBB thiolate to the reaction medium at definite intervals and (iii) rapid cooling.

Optical properties of the parent Au_{25} QCs were modified upon forming the red-emitting cluster (labelled as Au_{29} in the figure; nuclearity explained later), as depicted in Fig. 1. Though a dampening of the characteristic absorption features of Au_{25} clusters (black trace in Fig. 1A) was observed for the red-luminescent clusters (red trace), a distinct shoulder at 707 nm was observed in the case of the latter (see Fig. S3†). The dampening could be due to the increased charges on the cluster surface due to thiolate attachment.[9] Photographs taken under UV light (inset of Fig. 1B) clearly show the drastic change in the visible luminescence of parent $Au_{25}SBB_{18}$ and red-luminescent clusters. Photoluminescence spectra for both the clusters at excitation wavelengths, 467 (thick line) and 992 nm (thin line), respectively are shown in Fig. 1B. Parent $Au_{25}SBB_{18}$ emits primarily in the NIR region (see Fig. S1C†) with a peak maximum at 1030 nm (black thin line in Fig. 1B) while the red-emitting cluster showed an emission maximum at 737 nm (red thick line) with a concomitant loss of NIR emission. The fluorescence QY of the resultant red luminescent cluster was calculated to be 1.8% in THF medium at room temperature. This was much higher than that of parent $Au_{25}SBB_{18}$ clusters (0.04%) and that reported for other organic thiolate ligand protected Au_{25} clusters.[9,19–21] Fig. S4† compares the NIR emission (excited at 992 nm) from the parent $Au_{25}SBB_{18}$ QCs (green trace) and the resultant red luminescent clusters (blue trace). NIR emission from the red luminescent clusters is expanded (140 times, blue dotted line in Fig. S4†) for clarity. The absence of the prominent emission feature at 1030 nm (seen in parent Au_{25}) in the red luminescent cluster indicates the modification of the cluster. Identical concentrations of both the clusters are compared in the spectra, under similar instrumental conditions.

It is likely that the emergence of luminescence could be due to the core etching of the cluster by unreacted ligands as reported in earlier studies.[51–56] Core etching of nanoparticles/clusters in aqueous medium to form smaller clusters with luminescence is well known in the literature. However, this scenario can be ruled out in our case as the parent $Au_{25}SBB_{18}$ QCs exhibited high stability against core etching upon heating in the presence of excess BBSH. Intact optical absorption features of $Au_{25}SBB_{18}$ even in the presence of high thiol concentrations are observed in Fig. S1B.† Fig. S5A† shows the luminescence spectra of the solutions before and after addition of similar amounts of BBSH thiol (instead of Au(I)SBB thiolate) to the Au_{25} cluster, under identical reaction conditions. Though reports exist on the observation of luminescence from various Au(I) complexes in solution under different conditions,[8,57] this was ruled out in our case as heating the Au(I)SBB thiolate for 24 h under similar conditions also did not result in luminescent species (Fig. S5B†), validating that the observed luminescence was not from a Au(I)SBB thiolate. Moreover, comparison of the photoluminescence profile of the red luminescent cluster with identical concentrations (with respect to BBSH thiol) of precursor species validates its formation (Fig. S6†).

The red-emitting cluster could be successfully separated by preparative thin layer chromatography (TLC) with dichloromethane in hexane as the eluent (inset of Fig. 2A). TLC as a methodology for separating clusters has been reported earlier.[58] It is important to have pure QCs in order to determine their molecularity using mass spectrometric techniques. Both the clusters contain a certain amount of free BBSH which is observed as a blue band on the TLC plate, under UV light. Fig. S7† shows the SEM and EDAX images of a TLC plate with the separated red luminescent fraction. Photographs of the plate under UV and visible light (a and a′ in Fig. S7†) show the distinct luminescence.

Electrospray ionization mass spectrometry (ESI MS) has been considered as a reliable spectroscopic technique for the precise characterization of the cluster in the absence of crystal structures. Fig. S8A† compares the ESI mass spectra, in the negative ion mode, collected from the parent $Au_{25}SBB_{18}$ QCs (black trace) and the red luminescent cluster (red trace). In the case of the red luminescent cluster (Fig. 2A), apart from a peak at m/z 8152 (marked with a *) corresponding to the parent $Au_{25}SBB_{18}$ species, three intense peaks at m/z 4467, 4656 and 4844 were observed (region marked with a # in Fig. 2A). Fig. S8B† shows an expanded view of the region marked with the symbol, # in Fig. 2A. A difference of m/z 188 between the peaks, corresponding to (Au + SBB)/2, was observed between the three peaks marked with i, ii and iii in Fig. 2A. The isotope separation seen in each of the peaks is m/z 0.5, suggesting a dianion. From a theoretical prediction and isotope distribution, the peaks were assigned to $[Au_{27}(SBB)_{20}S]^{2-}$, $[Au_{28}(SBB)_{21}S]^{2-}$ and $[Au_{29}(SBB)_{22}S]^{2-}$ corresponding to $[Au_nSBB_nS]^{2-}$ (n = 2–4) in addition to $Au_{25}SBB_{18}$. The almost equal intensity of the three species indicates that they are formed as a result of fragmentation of a single species, due to asymmetric cleavage of similar bonds, rather than the formation of individual species in solution.

Evidence of the thiolate shell was obtained from matrix-assisted laser desorption ionization (MALDI) mass spectrometry as well (green trace in Fig. 2B). Though weak features were observed after 12 h, distinct peaks corresponding to the addition of the $[S(AuSBB)_n]$ unit to $Au_{25}SBB_{18}$ QC emerged after 24 h of the reaction (black to green trace in Fig. 2B). The peaks were separated by a mass difference of m/z 376 corresponding to a unit of (Au + SBB) and the highest peak was $Au_{29}SBB_{22}S$. This is in agreement with ESI MS data shown in Fig. 2A. Time dependent MALDI measurements confirmed that the red luminescent cluster, henceforth termed as Au_{29},

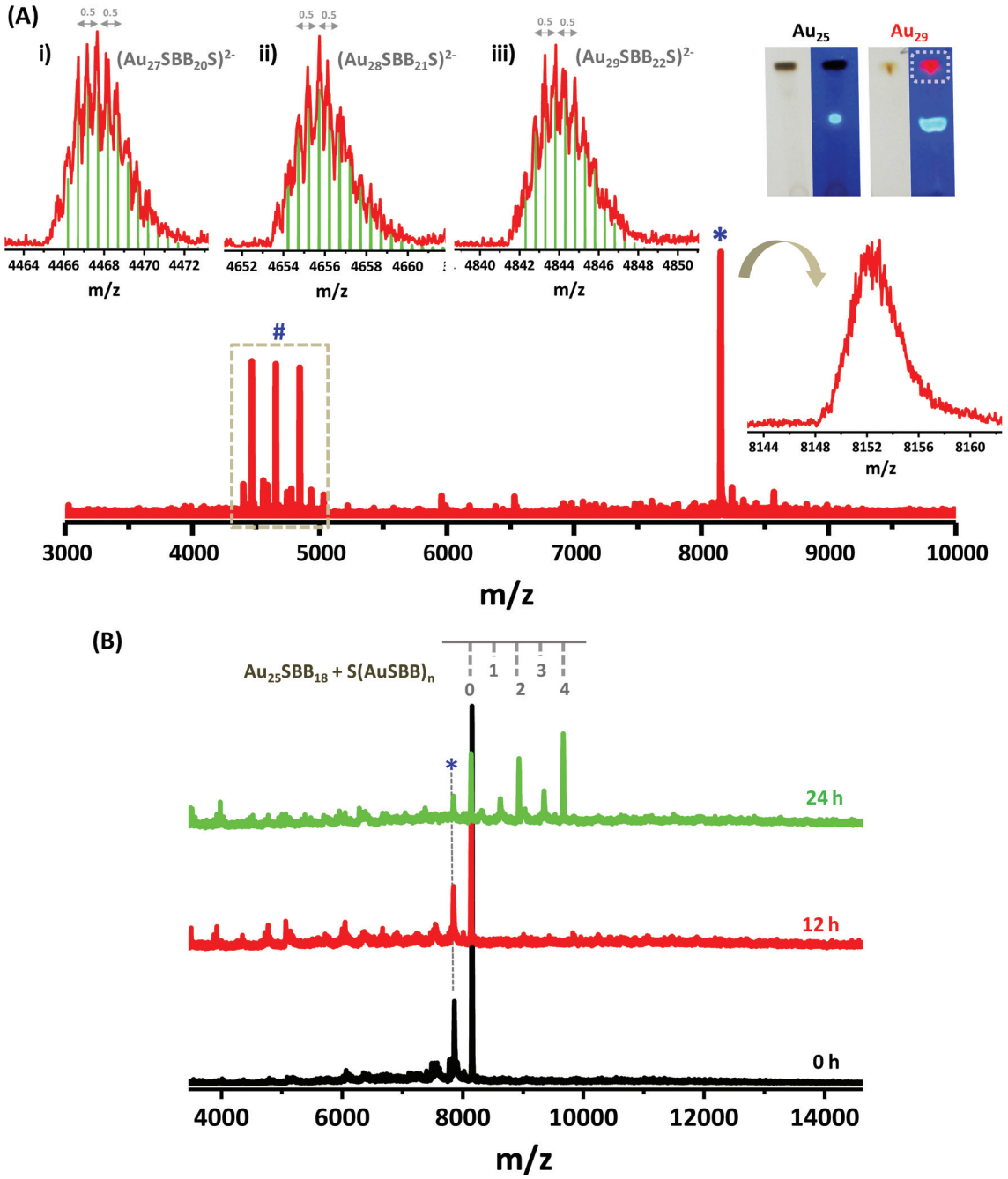

Fig. 2 ESI MS (A) and time dependent evolution of MALDI mass spectra (B) in negative ion mode of the red luminescent Au_{29} cluster. The three prominent peaks (marked with a #) apart from parent $Au_{25}SBB_{18}$ (marked with a * and expanded to depict the isotopic distribution corresponding to −1 charge) are expanded in insets (i–iii). The green lines in (i–iii) are the simulated isotope patterns for (i) $[Au_{27}(SBB)_{20}S]^{2-}$, (ii) $[Au_{28}(SBB)_{21}S]^{2-}$, and (iii) $[Au_{29}(SBB)_{22}S]^{2-}$. Peak separation of *m*/*z* 0.5 is marked in the experimental spectra. The inset of (A) also shows the TLC separation of parent Au_{25} and the red luminescent Au_{29} cluster (marked with a dotted circle) eluted with a DCM/hexane mixture (80 : 20) as the eluent. Fragmentation due to the C–S cleavage of the SBB ligand from Au_{25} (marked with an asterisk in B) is also observed.

was formed in solution only after prolonged heating. DCTB was used as the matrix for all measurements. Careful control over the laser power was crucial to observe the peaks without further fragmentation. The additional sulphur present in the cluster is suggestive of an unusual ligand structure. However, the cleavage of the R–S bond is observed in clusters[45,59] and crystal structures with additional sulphur atoms.[60] Moreover, Ag_2S clusters have been formed from $Ag_{25}SR_{18}$ clusters[61] in solution which occurs especially at temperatures used here. Thus, we believe that such clusters of the kind suggested are possible. Recently, an AIE mechanism has been proposed for water soluble glutathione protected Au[8,49] and bimetallic

Au/Ag clusters[50] wherein luminescence properties of the clusters are thought to involve the long Au(I)–thiolate motifs on the cluster surface. While ESI MS shows the formation of clusters larger than Au_{25} in solution, photoluminescence data from the cluster solutions showed a blue shift in the peak maximum for Au_{29} QCs compared to parent $Au_{25}SBB_{18}$. As the charge density has a critical role in the enhancement of luminescence in the QCs,[9,10] we proceeded to identify the role of the charge state of Au_{25} QCs in organic media. Unlike Ag clusters, surface oxidation is difficult in Au_{25} QCs. But, it is likely that partial oxidation of the thiolate staples (Au_2L_3) on the Au_{13} core can modify their overall charge.

In view of the critical role of surface charge density on the emergence of fluorescence in Au_{29}, X-ray photoelectron spectra (XPS) of parent Au_{25} and red-emitting Au_{29} clusters were recorded. The presence of surface thiolates in Au_{29} was also evident from the XPS spectra of the two clusters (Fig. 3). Though Au appears to exist in the near metallic (Au^0) state in both QCs as shown by the binding energy values of $4f_{7/2}$, a slight shift (0.4 eV) towards a higher binding energy value is noted for the Au_{29} species (84.7 eV) relative to the parent Au_{25} QC (84.3 eV). Note that binding energy values for Au $4f_{7/2}$ peaks are at 85.4 eV and 84.0 eV for Au^{+1} and Au^0, respectively.[62] Though small amounts of Au(I) are found on thiolate protected QCs,[63,64] the observed shift indicates the higher percentage of Au(I) in the Au_{29} cluster compared to parent Au_{25}. This clearly suggests the existence of oxidized thiolate staples on the cluster surface. The S $2p_{3/2}$ peak, seen at 163.1 eV (Au_{25}) and 162.8 eV (red luminescent species), for both clusters supports the Au–S thiolate binding to the core[65] and confirms the existence of only one type of S. On the basis of the above results, the enhanced luminescence in $Au_{25}SBB_{18}$ upon heating could be attributed

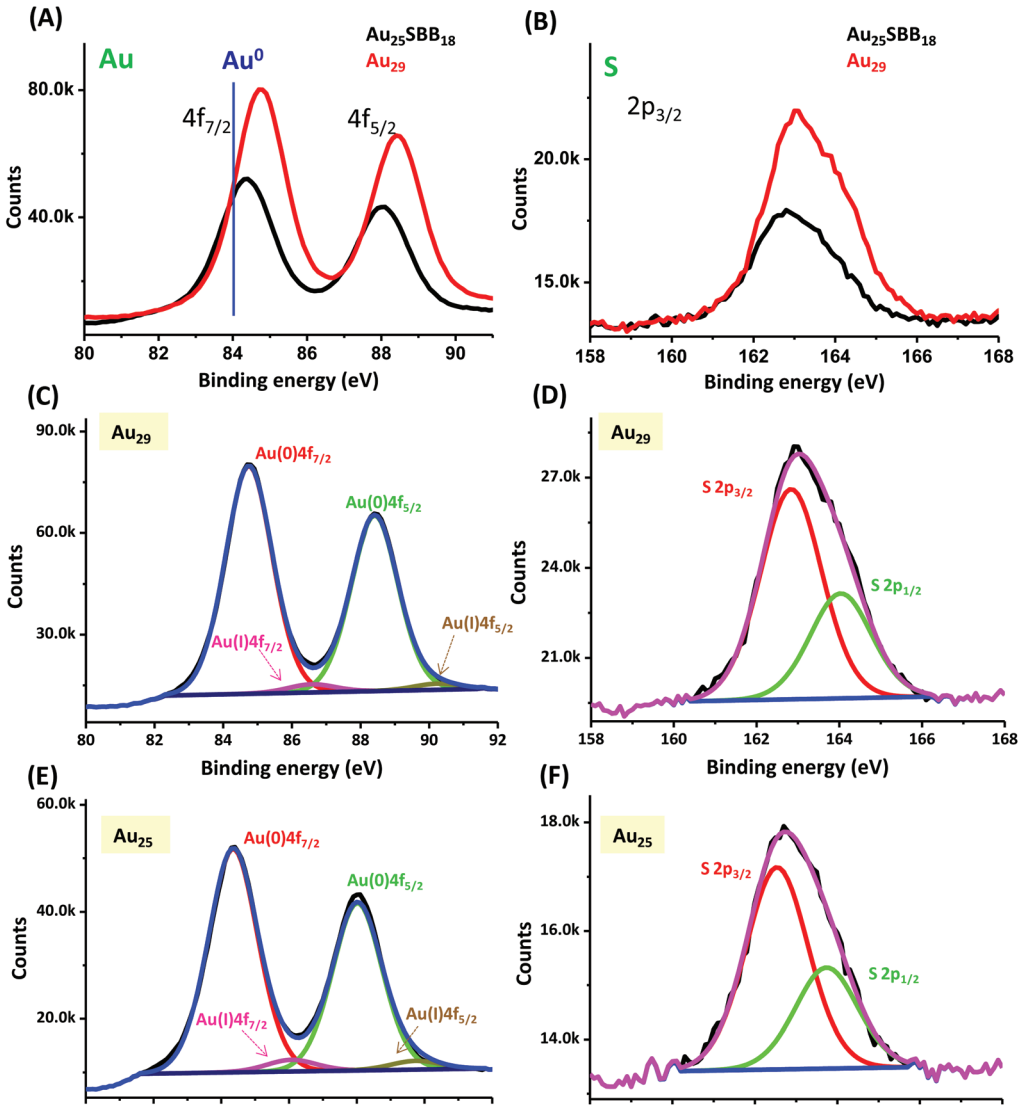

Fig. 3 XPS spectra of Au 4f (A) and S 2p (B) regions in parent $Au_{25}SBB_{18}$ (black trace) and luminescent Au_{29} (red trace) clusters. The blue line in (A) indicates the position of Au(0) at 84.0 eV. Deconvoluted XPS spectra of Au 4f (C, E) and S 2p (D, F) regions of the red luminescent Au_{29} clusters (C, D) and parent $Au_{25}SBB_{18}$ clusters (E, F) are also shown.

to the charge transfer from the oxidized surface thiolate ligands to the core of QC through the Au–S bonds and direct donation of delocalized electrons from electron-rich ligands to the metal core, as described by Jin *et al.*[9]

The presence of the thiolate shell around the cluster surface was further verified by thermogravimetric analysis (TGA). The red-emitting Au_{29} QCs showed higher organic content (observed metal to the organic content ratio (57.9% : 42.0%)), than the parent Au_{25} (60.2% : 39.7%) (Fig. S9†). The observed value was in accordance with the theoretical prediction, confirming the existence of the $Au_{29}SBB_{22}S$ cluster. Additional data were collected which further supported the proposed composition. A slight increase in the average size of the cluster was observed in the transmission electron microscopy (TEM) images of the red luminescent Au_{29} QCs compared to parent Au_{25} QCs (Fig. S10†). Au_{29} QCs also showed a tendency to aggregate. Compared to Au_{25} QCs (Fig. S10A†) which were well separated on the TEM grid, Au_{29} QCs (Fig. S10B†) showed a tendency to aggregate and exist as islands throughout the TEM grid. Note that this cannot be an effect of electron beam-induced aggregation, a common phenomenon observed in other Ag and Au clusters, as we observed no such effect on Au_{25} QCs. Scanning electron microscopic (SEM) images of the clusters at various stages of the reaction (Fig. S11A and B†) also show distinct changes in morphology. While a powdery texture is usually observed in the case of parent Au_{25} clusters (marked with a green circle in Fig. S11A†), an amorphous nature was observed for the purified red luminescent Au_{29} cluster (Fig. S11B†). Energy-dispersive analyses of X-ray (EDAX) mapping and spectra confirmed the presence of the constituent elements in the cluster (Fig. S11C†) and an Au/S ratio of 1 : 0.79 was seen in agreement with $Au_{29}SBB_{22}S$.

The presence of surface thiolates in red luminescent Au_{29} QCs was further confirmed by the addition of dilute sodium borohydride to the QCs (Fig. S12†). A drastic quenching of its visible luminescence accompanied by a significant red shift was observed upon addition of increasing amounts of sodium borohydride to the red luminescent Au_{29} QCs (black to tan trace in Fig. S12A†). The plot shown in Fig. S12B† compares the effect of similar amounts of $NaBH_4$ on parent Au_{25} QCs under identical conditions. Though a reduction in the luminescence intensity is noted in the case of parent Au_{25} QCs as well (red trace in Fig. S12B†), quenching is greater in the case of the Au_{29} species (black trace). This could be attributed to the reduction of the thiolate shell by sodium borohydride and consequent reduction in the overall surface charge of the cluster.

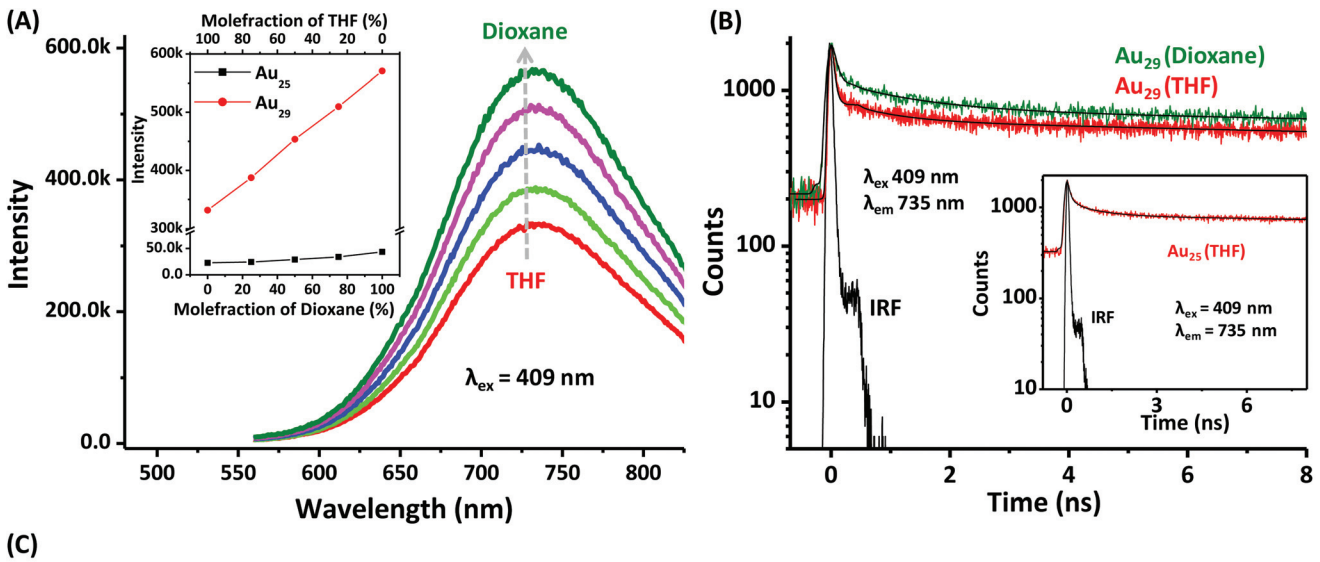

(C)

System	τ_1(%) ns	τ_2(%) ns	τ_3(%) ns	τ_{avg} (ns)
Au_{29} (THF)	0.05(84)	0.79(8.5)	35(7.5)	2.77
Au_{29} (1, 4-dioxane)	0.05(78)	1.08(10.5)	35(11.5)	4.20
Au_{25} (THF)	0.05(77)	0.91(11.5)	35(11.5)	4.15
Au_{25} (1, 4-dioxane)	0.06(77)	0.95(10)	34(13)	4.42

Fig. 4 (A) Emission spectra of Au_{29} QC in THF–1,4 dioxane mixture with different mole fractions of THF. The inset compares the corresponding emission spectra of Au_{25} QC in THF–1,4 dioxane solvent mixtures (see the text). (B) Picosecond-resolved decay transients of Au_{29} at 735 nm (ex 409 nm) in both THF and 1,4-dioxane solvents. The corresponding transients for Au_{25} in THF are shown as an inset. (C) Data corresponding to the picosecond time-resolved luminescence transients of Au_{29} and Au_{25} in pure THF and 1,4-dioxane.

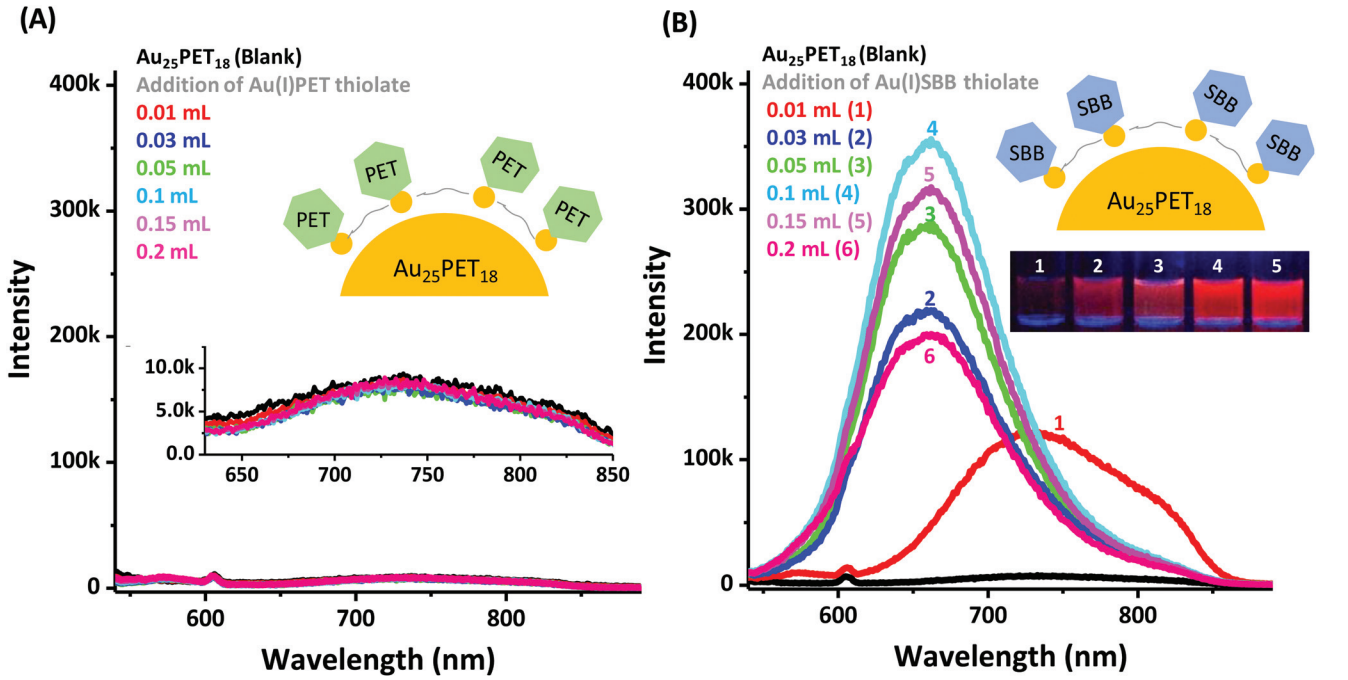

Fig. 5 Changes in emission spectra (λ_{ex} 514 nm) of $Au_{25}PET_{18}$ QCs upon reaction with various amounts of Au(I)PET thiolate (A) and Au(I)SBB thiolate (B). The inset of (B) shows the photographs of the cluster solution under conditions indicated in the figure. The inset also shows a cartoonic representation of the thiolate shell above $Au_{25}PET_{18}$ QCs.

The zeta potential of the parent $Au_{25}SBB_{18}$ QCs and the red luminescent Au_{29} QCs was determined to be −70.1 mV and +0.04 mV at room temperature, respectively. This enhanced charge is in accordance with the thiolate shell over the surface of $Au_{25}SBB_{18}$.

We conjectured that enhanced charge transfer in Au_{29} due to the thiolate shell, compared to that in Au_{25} could be responsible for the enhancement. To confirm this, we have performed solvent dependent luminescence studies on both the QCs. As shown in Fig. 4A, the luminescence from the Au_{29} cluster in 1,4-dioxane is significantly enhanced compared to that in THF. The enhancement is found to be linear upon increasing the concentration of 1,4-dioxane in THF–dioxane binary mixture. It has to be noted that the dielectric constant of the system can be varied from 7.58 (THF) to 2.25 (1,4-dioxane). The inset of Fig. 4A illustrates the relatively less sensitivity of Au_{25} QCS towards the polarity of the binary mixture of the host solvent. The observations suggest the higher extent of charge transfer in the case of Au_{29} QCs in comparison with Au_{25}.

In order to investigate non-radiative processes associated with the increased polarity of the host solvent of the QC, we performed picosecond resolved fluorescence studies (Fig. 4B) and the corresponding time scales are tabulated in the table (Fig. 4C). Au_{29} QCs show tri-exponential fluorescence relaxation with time constants of 50 ps (84%), 790 ps (8.5%), and 35 ns (7.5%) in THF. Faster and slower time constants are found to be similar in pure 1,4-dioxane. Interestingly, the second time constant of 790 ps in THF is slowed down to 1.08 ns in 1,4-dioxane, revealing that the key time scale accounts for the charge transfer dynamics, which is the consequence of change in polarity.[66] While the slowest component (35 ns) accounts for the radiative life time of the QC HOMO–LUMO transition,[67,68] the fastest component of 50 ps can be rationalised to thermalization dynamics in the QC[69] which depends upon the energy of excitation. We have performed excitation dependent picosecond resolved studies using various excitation lasers (409 nm, 510 nm and 635 nm) and found that the fastest component is gradually decreased with the increase in excitation wavelengths, revealing the vanishing of small contribution of thermalization dynamics at 635 nm excitation (Fig. S14†). We have calculated the non-radiative rate in the case of THF with reference to 1,4-dioxane following the equation,[70]

$$k_{nr} = \frac{1}{\langle \tau \rangle} - \frac{1}{\langle \tau_0 \rangle}$$

and found it to be 1.2×10^8 s^{-1}. As shown in Fig. 4B, inset, the temporal characteristic of the Au_{25} cluster shows insignificant dependency on the polarity of the host solvent. Thus the contribution of the charge transfer effect in Au_{29} QCs in comparison with parent Au_{25} QCs is confirmed.

The mechanism of increased surface charge responsible for visible luminescence enhancement was verified with the help of other experiments illustrated below. These experiments were intended to prove the possibility of ligand structure-induced changes in luminescence and not to establish the

nature of the metal core or composition of the resulting clusters. Heating $Au_{25}SBB_{18}$ cluster loaded silica gel at 55 °C (brown colored solid, see photographs shown in Fig. S14†) showed luminescence (for 24 h). Photographs of the $Au_{25}SBB_{18}$-loaded silica gel before and after heat treatment are shown in the figure. Though no red luminescence was observed from the material before heat treatment, a bright red emission was observed from the silica gel after 24 h of heating in a sand bath (set-up is shown in Fig. S14†). This confirms that the observed luminescence was not a result of solution state dynamics involving other species in solution as solid cluster samples were heated in this case. Here, instead of Au(I) thiolate, silica having hydroxyl groups on its surface may be acting as an electron donor leading to charge transfer and thus causing luminescence enhancement of the adsorbed Au_{25} QCs.

Further, this strategy is also illustrated for yet another hydrophobic Au_{25} QC with phenylethanethiol as the protecting ligand. The $Au_{25}PET_{18}$ cluster was chosen as it is a well-studied and characterized system with known crystal structure.[26,27] Advantages of a solved X-ray crystal structure in the case of $Au_{25}PET_{18}$ has triggered a lot of studies in catalysis, chirality, magnetism, *etc*., involving these clusters which make use of the structure–property correlations to understand their unique properties. Imparting visible luminescence on such materials can add another dimension to these studies. Fig. 5 shows variation in the emission spectra of $Au_{25}PET_{18}$ QCs upon heating with two different thiolates namely, Au(I)PET (Fig. 5A) and Au(I)SBB (Fig. 5B). Interestingly, a 35 times enhancement in luminescence was observed in the case of the cluster treated with Au(I)SBB thiolate compared to PET thiolate. While addition of Au(I)PET thiolate showed little or no change in the emission intensities of the parent clusters at an excitation of 514 nm, similar amounts of SBB thiolate resulted in drastic enhancement in emission (black to cyan trace in Fig. 5B). The stronger electron donating capability of the BBSH ligand (Ph(*tert*-butyl)CH_2– group) compared to PET (PhC_2H_4– group) might be the reason for this enhancement. Emergence of bright red luminescence in solution is evident from the photographs of the cluster (inset of Fig. 5B). Images 1–5 show increasing amounts of Au(I)SBB thiolate in solution.

Experimental

Materials and methods

Tetrachloroauric(III) acid ($HAuCl_4{\cdot}3H_2O$) and methanol were purchased from SRL Chemical Co. Ltd, India. 4-(*t*-Butyl)benzyl mercaptan $(CH_3)_3C–C_6H_4–CH_2SH$ (BBSH), 2-phenylethanethiol $C_6H_5–CH_2–CH_2SH$ (PET) and sodium borohydride ($NaBH_4$) were purchased from Sigma Aldrich. Silica gel (60–120 mesh) was obtained from Merck, India. Tetrahydrofuran was purchased from Rankem, India. All chemicals were analytical grade and were used without further purification. Glassware was cleaned thoroughly with aqua regia (HCl/HNO_3, 3 : 1 vol%), rinsed with distilled water, and dried in an oven prior to use. Triply distilled water was used throughout the experiments.

Synthesis of $Au_{25}SBB_{18}$ and the red luminescent Au_{29} cluster

$Au_{25}SBB_{18}$ was synthesized as per our earlier report.[6] Briefly, 10 mL $HAuCl_4{\cdot}3H_2O$ (14.5 mM in THF) was added to 15 mL BBSH thiol (89.2 mM in THF) while stirring at 400 rpm at room temperature (29 °C) in a round bottom flask. The solution becomes colorless after 15 min, indicating the formation of the Au(I)SBB thiolates. An aqueous solution of 2.5 mL $NaBH_4$ (0.4 M) was added rapidly to the reaction mixture under vigorous stirring (1100 rpm) and the solution turned from colorless to black, indicating the formation of clusters. The reaction was allowed to proceed with constant stirring for 3 h under ambient conditions and then for 3 h at 45 °C. The solution was left overnight to yield monodisperse species. The THF solvent was removed under vacuum and the residue was washed repeatedly with a 1 : 1 water : methanol mixture to remove excess BBSH thiol and other side products. The Au_{25} cluster thus precipitated was dried and used for further experiments. The red luminescent Au_{29} clusters were synthesized *via* thermal treatment of Au_{25} clusters followed by rapid cooling. Approximately 10 mg of purified, solid $Au_{25}SBB_{18}$ (used as the precursor) was dissolved in 3 mL THF and 3 mL water. The cluster phase is separated from the organic layer and the aqueous layer remains colorless. The solution was heated at 55 °C for 24 h with stirring in a sealed container. After 12 h, 0.6 mL of Au(I)SBB thiolate was added to the reaction mixture and the reaction was allowed to proceed for another 12 h. Afterwards, the dark reddish brown upper (organic) layer was collected and cooled to 4 °C for 4 h. Visible bright red luminescence was observed from the cluster after this cooling step. Later the solvent was removed under vacuum and the residue was washed repeatedly with 1 : 1 water/methanol mixture and dried. To synthesize the thiolate, 8 mL $HAuCl_4{\cdot}3H_2O$ (13 mM in THF) was dissolved in 5 mL THF and to this solution 20 μL BBSH thiol (1 : 1 ratio of Au^{3+} and BBSH thiol) was added while stirring at 300 rpm at room temperature (29 °C). The solution was allowed to equilibrate for 12 h before use.

TLC separation

The cluster samples (both Au_{25} and Au_{29}) in THF medium (2 mg in 0.3 mL) were pipetted (1 μL each) to the TLC plates and dried in air. After drying, the plate was eluted with a DCM/hexane mixture (the optimal solvent ratio varies with the cluster system[58]). In our case an 80 : 20 mixture of DCM : hexane was used as the eluent. After the separation, the bands were cut from the TLC plate, and the clusters from each band were extracted separately and analyzed. The solid pieces of the TLC plate were removed from these extracts *via* centrifugation.

Instrumentation

Mass spectral studies were carried out using a Voyager DE PRO biospectrometry workstation (Applied Biosystems) matrix-assisted laser desorption ionization (MALDI) time-of-flight (TOF) mass spectrometer in the linear mode as well as using a

MALDI TOF/TOF (UltrafleXtreme, Bruker Daltonics) mass spectrometer. In the case of MALDI TOF MS, a pulsed nitrogen laser of 337 nm was used (a maximum firing rate, 20 Hz; a maximum pulse energy, 300 μJ) for the measurements. The MALDI TOF/TOF mass spectrometer utilizes a 1 kHz smartbeam-II laser, FlashDetector system, and a minimum 4 GHz digitizer. Mass spectra were recorded in positive and negative ion modes and were averaged for 500–700 shots. DCTB (*trans*-2-[3-(4-*t*-butylphenyl)-2-methyl-2-propenylidene]malononitrile) was used as the matrix for all MALDI MS measurements. All spectra were recorded at a threshold laser intensity to keep fragmentation to a minimum. The concentration of the analyte and the mass spectral conditions (laser intensity and spectrometer tune files) were optimized to obtain good quality spectra. UV-vis absorption spectra were recorded using a Perkin-Elmer Lambda 25 spectrophotometer. The experiments were carried out at room temperature, and the absorption spectra were recorded from 200 to 1100 nm. Luminescence measurements were carried out on a Jobin Yvon NanoLog instrument. The band pass for excitation and emission was set at 3 nm. QYs were measured using cluster solutions of appropriate dilutions (~0.04 OD absorption at 467 nm) using $[Au_{25}PET_{18}]^-$ as a reference (QY 0.01% as reported previously[9]). All picosecond-resolved fluorescence decay transients were measured by using a commercially available spectrophotometer (Life Spec-ps, Edinburgh Instruments, UK) with 90 ps instrument response function (IRF). The excitations at 409 nm, 510 nm and 635 nm were obtained using a pulse laser diode from PicoQuant, Germany. The observed fluorescence transients were fitted by using a nonlinear least squares fitting procedure to a function $\left(X(t) = \int_0^t E(t')R(t-t')\mathrm{d}t'\right)$ comprising of convolution of the IRF $(E(t))$ with a sum of exponential $\left(R(t) = A + \sum_{i=1}^{N} B_i \mathrm{e}^{-t/\tau_i}\right)$ with pre-exponential factors (B_i), characteristic lifetimes (τ_i) and a background (A). The relative concentration in a multi exponential decay was finally expressed as:

$$c_n = \frac{B_n}{\sum_{i=1}^{N} B_i} \times 100$$

The quality of the curve fitting was evaluated by reduced chi-square and residual data. It has to be noted that with our time-resolved instrument, we can resolve at least one fourth of the instrument response time constants after the de-convolution of the IRF. The average lifetime (amplitude-weighted) of a multi-exponential decay is expressed as:

$$\tau_{av} = \sum_{i=1}^{N} c_i \tau_i$$

ESI mass spectrometric measurements were done in the negative mode using a Synapt G2 HDMS, quadrupole time-of flight (Q TOF), ion mobility, orthogonal acceleration mass spectrometer with electrospray ionization having a mass range of up to 32 kDa. The Synapt instrument used for ESI measurements combined an exact-mass quadrupole and a high resolution time-of-flight mass spectrometer with Triwave technology, enabling measurements in the TOF mode. The purified samples were dispersed in THF and used for both mass spectrometric measurements. The samples were electrosprayed at a flow rate of 5 μL min^{-1} and at a capillary temperature of 150 °C. The spectra were averaged for 80–100 scans. SEM and EDAX images were obtained using a FEI QUANTA-200 SEM. For the SEM and EDAX measurements, samples were either spotted or stuck (in the case of the TLC plate) on a carbon substrate and dried at ambient temperature. TEM was conducted using a JEOL 3011, using a 300 kV instrument with an ultra-high-resolution (UHR) polepiece. The samples were prepared by dropping the dispersion on amorphous carbon films supported on a copper grid and dried under laboratory conditions. The zeta potential measurements were carried out using a Malvern Zetasizer nz (M3-PALS) instrument.

Conclusions

In summary, an efficient method to enhance the visible luminescence in visibly non-luminescent organic-soluble Au_{25} QCs is developed. Our study demonstrates that making an additional shell of thiolate on the cluster surface can increase the surface charge density resulting in enhancement of the visible luminescence. The critical role of temperature in the emergence of luminescence in QCs has been studied in detail. The restoration of the surface ligand shell on the Au_{25} cluster and subsequent physicochemical modification to the cluster was probed by various mass spectral and spectroscopic techniques. This method has been successfully illustrated by imparting visible red luminescence in PET protected Au_{25} QCs. Our results provide fundamental insights into the ligand characteristics on the origin of luminescence in QCs.

Acknowledgements

We thank the Department of Science and Technology, Government of India (DST), for constantly supporting our research program on nanomaterials. A. M. thanks CSIR for a research fellowship. Dr Abdul Jaleel, Mr Arun Surendran and Mr M. Saravanakumar at Rajiv Gandhi Centre for Biotechnology (RGCB) are thanked for help in mass spectral measurements.

References

1 S. Choi, R. M. Dickson and J. Yu, *Chem. Soc. Rev.*, 2012, **41**, 1867–1891.
2 A. Mathew and T. Pradeep, *Part. Part. Syst. Charact.*, 2014, **31**, 1017–1053.
3 X. Yuan, Z. Luo, Y. Yu, Q. Yao and J. Xie, *Chem. – Asian J.*, 2013, **8**, 858–871.

4 A. Mathew, P. R. Sajanlal and T. Pradeep, *Angew. Chem., Int. Ed.*, 2012, **51**, 9596–9600.
5 J. Zheng, C. Zhou, M. Yu and J. Liu, *Nanoscale*, 2012, **4**, 4073–4083.
6 J. Zheng, C. Zhang and R. M. Dickson, *Phys. Rev. Lett.*, 2004, **93**, 077402.
7 A. Mathew, P. R. Sajanlal and T. Pradeep, *J. Mater. Chem.*, 2011, **21**, 11205–11212.
8 Z. Luo, X. Yuan, Y. Yu, Q. Zhang, D. T. Leong, J. Y. Lee and J. Xie, *J. Am. Chem. Soc.*, 2012, **134**, 16662–16670.
9 Z. Wu and R. Jin, *Nano Lett.*, 2010, **10**, 2568–2573.
10 G. Wang, R. Guo, G. Kalyuzhny, J.-P. Choi and R. W. Murray, *J. Phys. Chem. B*, 2006, **110**, 20282–20289.
11 G. Wang, T. Huang, R. W. Murray, L. Menard and R. G. Nuzzo, *J. Am. Chem. Soc.*, 2005, **127**, 812–813.
12 X. Tan and R. Jin, *Wiley Interdiscip. Rev.: Nanomed. Nanobiotechnol.*, 2013, **5**, 569–581.
13 C. V. Conroy, J. Jiang, C. Zhang, T. Ahuja, Z. Tang, C. A. Prickett, J. J. Yang and G. Wang, *Nanoscale*, 2014, **6**, 7416–7423.
14 T. Vosch, Y. Antoku, J.-C. Hsiang, C. I. Richards, J. I. Gonzalez and R. M. Dickson, *Proc. Natl. Acad. Sci. U. S. A.*, 2007, **104**, 12616–12621.
15 J. Xie, Y. Zheng and J. Y. Ying, *J. Am. Chem. Soc.*, 2009, **131**, 888–889.
16 X. Yuan, Z. Luo, Q. Zhang, X. Zhang, Y. Zheng, J. Y. Lee and J. Xie, *ACS Nano*, 2011, **5**, 8800–8808.
17 S.-I. Tanaka, J. Miyazaki, D. K. Tiwari, T. Jin and Y. Inouye, *Angew. Chem., Int. Ed.*, 2011, **50**, 431–435.
18 A. Das, T. Li, G. Li, K. Nobusada, C. Zeng, N. L. Rosi and R. Jin, *Nanoscale*, 2014, **6**, 6458–6462.
19 R. Jin, *Nanoscale*, 2010, **2**, 343–362.
20 J. F. Parker, C. A. Fields-Zinna and R. W. Murray, *Acc. Chem. Res.*, 2010, **43**, 1289–1296.
21 G. Wang, T. Huang, R. W. Murray, L. Menard and R. G. Nuzzo, *J. Am. Chem. Soc.*, 2004, **127**, 812–813.
22 A. Verma, O. Uzun, Y. Hu, Y. Hu, H.-S. Han, N. Watson, S. Chen, D. J. Irvine and F. Stellacci, *Nat. Mater.*, 2008, **7**, 588–595.
23 C. M. Jewell, J.-M. Jung, P. U. Atukorale, R. P. Carney, F. Stellacci and D. J. Irvine, *Angew. Chem., Int. Ed.*, 2011, **50**, 12312–12315.
24 H.-Y. Lee, S. H. R. Shin, L. L. Abezgauz, S. A. Lewis, A. M. Chirsan, D. D. Danino and K. J. M. Bishop, *J. Am. Chem. Soc.*, 2013, **135**, 5950–5953.
25 E. A. Appel, M. W. Tibbitt, M. J. Webber, B. A. Mattix, O. Veiseh and R. Langer, *Nat. Commun.*, 2014, **6**, 6295, DOI: 10.1038/ncomms7295.
26 M. W. Heaven, A. Dass, P. S. White, K. M. Holt and R. W. Murray, *J. Am. Chem. Soc.*, 2008, **130**, 3754–3755.
27 M. Zhu, C. M. Aikens, F. J. Hollander, G. C. Schatz and R. Jin, *J. Am. Chem. Soc.*, 2008, **130**, 5883–5885.
28 T. Dainese, S. Antonello, J. A. Gascon, F. Pan, N. V. Perera, M. Ruzzi, A. Venzo, A. Zoleo, K. Rissanen and F. Maran, *ACS Nano*, 2014, **8**, 3904–3912.
29 Y. Zhu, H. Qian, B. A. Drake and R. Jin, *Angew. Chem., Int. Ed.*, 2010, **49**, 1295–1298.
30 D. R. Kauffman, D. Alfonso, C. Matranga, H. Qian and R. Jin, *J. Am. Chem. Soc.*, 2012, **134**, 10237–10243.
31 X. Nie, H. Qian, Q. Ge, H. Xu and R. Jin, *ACS Nano*, 2012, **6**, 6014–6022.
32 S. Yamazoe, K. Koyasu and T. Tsukuda, *Acc. Chem. Res.*, 2014, **47**, 816–824.
33 K. Kwak and D. Lee, *J. Phys. Chem. Lett.*, 2012, **3**, 2476–2481.
34 M. Zhu, C. M. Aikens, M. P. Hendrich, R. Gupta, H. Qian, G. C. Schatz and R. Jin, *J. Am. Chem. Soc.*, 2009, **131**, 2490–2492.
35 S. Antonello, N. V. Perera, M. Ruzzi, J. A. Gascón and F. Maran, *J. Am. Chem. Soc.*, 2013, **135**, 15585–15594.
36 M. Zhu, H. Qian, X. Meng, S. Jin, Z. Wu and R. Jin, *Nano Lett.*, 2011, **11**, 3963–3969.
37 Y. Negishi, K. Munakata, W. Ohgake and K. Nobusada, *J. Phys. Chem. Lett.*, 2012, **3**, 2209–2214.
38 W. Kurashige, K. Munakata, K. Nobusada and Y. Negishi, *Chem. Commun.*, 2013, **49**, 5447–5449.
39 D. R. Kauffman, D. Alfonso, C. Matranga, H. Qian and R. Jin, *J. Phys. Chem. C*, 2013, **117**, 7914–7923.
40 C. Kumara, C. M. Aikens and A. Dass, *J. Phys. Chem. Lett.*, 2014, **5**, 461–466.
41 Y. Negishi, W. Kurashige, Y. Niihori, T. Iwasa and K. Nobusada, *Phys. Chem. Chem. Phys.*, 2010, **12**, 6219–6225.
42 A. Tlahuice-Flores, R. L. Whetten and M. Jose-Yacaman, *J. Phys. Chem. C*, 2013, **117**, 20867–20875.
43 Y. Niihori, M. Matsuzaki, T. Pradeep and Y. Negishi, *J. Am. Chem. Soc.*, 2013, **135**, 4946–4949.
44 E. S. Shibu, M. A. H. Muhammed, T. Tsukuda and T. Pradeep, *J. Phys. Chem. C*, 2008, **112**, 12168–12176.
45 A. Mathew, G. Natarajan, L. Lehtovaara, H. Häkkinen, R. M. Kumar, V. Subramanian, A. Jaleel and T. Pradeep, *ACS Nano*, 2014, **8**, 139–152.
46 J. Akola, M. Walter, R. L. Whetten, H. Häkkinen and H. Grönbeck, *J. Am. Chem. Soc.*, 2008, **130**, 3756–3757.
47 S. H. Yau, O. Varnavski and T. Goodson, *Acc. Chem. Res.*, 2013, **46**, 1506–1516.
48 M. S. Devadas, J. Kim, E. Sinn, D. Lee, T. Goodson and G. Ramakrishna, *J. Phys. Chem. C*, 2010, **114**, 22417–22423.
49 Y. Yu, Z. Luo, D. M. Chevrier, D. T. Leong, P. Zhang, D.-e. Jiang and J. Xie, *J. Am. Chem. Soc.*, 2014, **136**, 1246–1249.
50 X. Dou, X. Yuan, Y. Yu, Z. Luo, Q. Yao, D. T. Leong and J. Xie, *Nanoscale*, 2014, **6**, 157–161.
51 M. A. Habeeb Muhammed, P. K. Verma, S. K. Pal, A. Retnakumari, M. Koyakutty, S. Nair and T. Pradeep, *Chem. – Eur. J.*, 2010, **16**, 10103–10112.
52 L. Dhanalakshmi, T. Udayabhaskararao and T. Pradeep, *Chem. Commun.*, 2011, **48**, 859–861.
53 I. Díez, M. Pusa, S. Kulmala, H. Jiang, A. Walther, A. S. Goldmann, A. H. E. Müller, O. Ikkala and R. H. A. Ras, *Angew. Chem., Int. Ed.*, 2009, **48**, 2122–2125.

54 C.-Y. Ke, T.-H. Chen, L.-C. Lu and W.-L. Tseng, *RSC Adv.*, 2014, **4**, 26050–26056.
55 X. Le Guével, V. Trouillet, C. Spies, G. Jung and M. Schneider, *J. Phys. Chem. C*, 2012, **116**, 6047–6051.
56 M. A. H. Muhammed, F. Aldeek, G. Palui, L. Trapiella-Alfonso and H. Mattoussi, *ACS Nano*, 2012, **6**, 8950–8961.
57 D. V. Krupenya, P. A. Snegurov, E. V. Grachova, V. V. Gurzhiy, S. P. Tunik, A. S. Melnikov, P. Y. Serdobintsev, E. G. Vlakh, E. S. Sinitsyna and T. B. Tennikova, *Inorg. Chem.*, 2013, **52**, 12521–12528.
58 A. Ghosh, J. Hassinen, P. Pulkkinen, H. Tenhu, R. Ras and T. Pradeep, *Anal. Chem.*, 2014, **86**, 12185–12190.
59 I. Chakraborty, A. Govindarajan, J. Erusappan, A. Ghosh, T. Pradeep, B. Yoon, R. L. Whetten and U. Landman, *Nano Lett.*, 2012, **12**, 5861–5866.
60 H. Yang, Y. Wang, A. J. Edwards, J. Yan and N. Zheng, *Chem. Commun.*, 2014, **50**, 14325–14327.
61 K. P. Remya, T. Udayabhaskararao and T. Pradeep, *J. Phys. Chem. C*, 2012, **116**, 26019–26026.
62 K. Chaudhari, P. L. Xavier and T. Pradeep, *ACS Nano*, 2011, **5**, 8816–8827.
63 P. D. Jadzinsky, G. Calero, C. J. Ackerson, D. A. Bushnell and R. D. Kornberg, *Science*, 2007, **318**, 430–433.
64 R. L. Whetten and R. C. Price, *Science*, 2007, **318**, 407–408.
65 G. J. Ashwell, B. Urasinska-Wojcik and L. J. Phillips, *Angew. Chem., Int. Ed.*, 2010, **49**, 3508–3512.
66 M. Zhou, S. Long, X. Wan, Y. Li, Y. Niu, Q. Guo, Q.-M. Wang and A. Xia, *Phys. Chem. Chem. Phys.*, 2014, **16**, 18288–18293.
67 X. Wen, P. Yu, Y.-R. Toh, A.-C. Hsu, Y.-C. Lee and J. Tang, *J. Phys. Chem. C*, 2012, **116**, 19032–19038.
68 E. S. Shibu and T. Pradeep, *Chem. Mater.*, 2011, **23**, 989–999.
69 P. F. Barbara, G. C. Walker and T. P. Smith, *Science*, 1992, **256**, 975–981.
70 S. Choudhury, S. Batabyal, T. Mondol, D. Sao, P. Lemmens and S. K. Pal, *Chem. – Asian J.*, 2014, **9**, 1395–1402.